Check for updates

Catalytic degradation of azo dyes by bimetallic nanoparticles loaded in smart polymer microgels†

Muhammad Arif ⓘD *

The contamination of water by azo dyes is increasing rapidly due to their waste use in textile industries. These dyes are very toxic for living things. Therefore, it is very important to remove these dyes from water. Various materials are reported for this purpose. Here, the most effective system of bimetallic nanoparticles in smart polymer microgels was prepared. The microgel system of *N*-isopropylmethacrylamide (NMA) (monomer) and methacrylic acid (MAa) (comonomer) was synthesized by a free radical precipitation polymerization method and then bimetallic (Ag/Ni) nanoparticles were encapsulated into the P(NMA-MAa) microgels by *in situ* reduction of both silver and nickel salts by $NaBH_4$ (reductant) after insertion of both (Ag^+/Ni^{2+}) ions. The P(NMA-MAa) microgels and Ag/Ni-P(NMA-MAa) hybrid microgels were characterized with FTIR, UV-vis, TGA, XRD, DLS, EDX, and STEM. The pH and temperature responsive behavior of Ag/Ni-P(NMA-MAa) was also evaluated. The catalytic efficiency of Ag/Ni-P(NMA-MAa) was assessed for degradation of methyl orange (MOr), congo red (CRe), eriochrome black T (EBlT) and methyl red (MRe) dyes under various conditions in aqueous medium. The apparent rate constant (k_0) value for MOr, CRe, EBlT and MRe was found to be 0.925 min^{-1}, 0.486 min^{-1}, 0.540 min^{-1} and 0.525 min^{-1} respectively. The Ag/Ni-P(NMA-MAa) was found to be an excellent recyclable catalyst.

1 Introduction

Purification of water is a hot topic of research nowadays because pollution of water is increasing day by day due to various applications of pollutants[1,2] and therefore, it is very difficult to get pure water. The main pollutants of wastewater are heavy metal ions,[2] nitroarenes,[3] pesticides[4] and toxic dyes.[5] Due to the vast scope of applications of organic dyes, they are the major component of wastewater as reported in the literature.[5–7] The azo dyes are the most stable toxic dyes. That is why the use of azo dyes is banned in different countries due to the severe toxic effect on human and aquatic life.[8] Therefore, it is a very important task to eliminate these toxic dyes from water.

Various types of materials such as metal organic frameworks,[9] ligands,[10] polymers,[11] metal nanoparticles[12] and metal nanoparticles loaded in microgels[13–18] are reported for the removal of azo dyes. The metal nanoparticles have advantage on metal organic frameworks, ligands, and polymers due to their high catalytic efficiency and recyclable property. But instability of metal nanoparticles is the only drawback. This drawback of metal nanoparticles can be controlled by using stabilizers such as surfactants,[19] polymers,[20] dendrimers[21] and microgels.[22] The

Department of Chemistry, School of Science, University of Management and Technology, Lahore 54770, Pakistan. E-mail: muhammadarif2861@yahoo.com; muhammadarif@umt.edu.pk

microgels are very efficient stabilizer to the metal nanoparticles. The encapsulation of metal nanoparticles in crosslinked network of polymer microgels are called hybrid microgels. The microgels, which shows stimuli responsive behavior, are called smart microgels. The smart microgels show swelling and deswelling behavior under different conditions of pH, temperature and ionic strength.[17] Different type of nanoparticles loaded into smart polymer microgels are reported in the literature.[23–25] From these metal nanoparticles, Ag nanoparticles along with low-cost metal nanoparticles loaded microgels have very much intension due to their high catalytic activity and cost effectiveness. The bimetallic nanoparticles loaded smart microgels[26,27] exhibit better catalytic activity than monometallic nanoparticles loaded system[28,29] because former system has synergistic effect. Therefore, bimetallic nanoparticles loaded into microgels is a hot topic of research now a days due to their excellent catalytic as well as responsive behavior of hybrid microgels.[30]

The catalytic performance of bimetallic nanoparticles loaded into smart microgels can be controlled by changing the temperature, pH, or ionic strength of the medium. The responsive behavior of hybrid microgels are mostly due to the presence of polar functional groups such as $-NH_2$, $-COOH$ and $-SO_3H$ in their structures. The catalytic activity of bimetallic nanoparticles loaded microgels is greater than monometallic nanoparticles loaded microgels. Saran *et al.*[31] also synthesized monometallic and bimetallic nanoparticles, and reported that

bimetallic nanoparticles have better catalytic activity than monometallic nanoparticles for degradation of organic dyes. The Ag nanoparticles along with costly noble metal nanoparticles in bimetallic nanoparticle systems have been reported frequently but rarely with cheap metal. The best of our knowledge, the synthesis, stimuli responsive behavior and catalytic efficiency of bimetallic (Ag/Ni) nanoparticles loaded in P(NMA-MAa) microgels is not reported in literature yet.

In the present work, poly(N-isopropylmethacrylamide-methacrylic acid) P(NMA-MAa) microgels were synthesized by free radical precipitation polymerization method (FRPPM) and then bimetallic (silver and nickel) nanoparticles were introduced into the sieves of crosslinked network of P(NMA-MAa) by in situ reduction method. The stability and stimuli responsive behavior of Ag/Ni-P(NMA-MAa) were also monitored by UV-visible spectrophotometry. The Ag/Ni nanoparticles loaded into P(NMA-MAa) systems were used as catalyst for degrade of MOr, MRe, EBlT and CRe dyes. The kinetics of catalytic degradation of azo dyes were also included in this study.

2 Experimental

2.1 Materials

NMA (98%), ammonium per sulfate (AS) (99%), N,N'-methylene bis acrylamide (MBA) (99%), sodium borohydride (NaBH$_4$) (98%), MAa (98%), sodium dodecyl sulfate (SDS) (98%), MOr, MRe, CRe, EBlT, silver nitrate (AgNO$_3$), nickel nitrate hexahydrate (Ni(NO$_3$)$_2$·6H$_2$O) (99.99%) were purchased from Sigma-Aldrich. Dialysis membrane was obtained from Scharlu.

2.2 Synthesis of P(NMA-MAa) and Ag/Ni-P(NMA-MAa)

1.196 g of NMA, 0.072 g of SDS, 0.046 g of MBA and 0.050 mL of MAa were added into a three-neck flask and then 95 mL deionized water (DI) into the flask and stirring for 30 min under N$_2$ supply. Then temperature increased up to 70 °C and maintained and then added 5 mL AS solution (0.08 M) and heated further for 5 h under N$_2$. Milky appearance was indicated the formation of P(NMA-MAa) microgels particles. After that the mixture was dialyzed for 5 days in a molecular porous spectator membrane with MNCO 12000–14000.

To synthesize Ag/Ni-P(NMA-MAa), 10 mL of P(NMA-MAa) were added into a three-neck flask and added slightly NaOH solution. The 3 mL of AgNO$_3$ (2 mM) and 3 mL of nickel nitrate (2 mM) were added and stirred for 30 min under N$_2$ at ambident temperature (26 °C). Then 5 mL of NaBH$_4$ (10 mM) was added into the reaction mixture and further stirred for 1 h. The color of mixture changed from milky to slightly brown which indicated the formation of nanoparticles into P(NMA-MAa). The product was dialyzed for 1 h.

2.3 Characterizations

The presence of different functionalities in P(NIPMA-MAA) and Ag/Ni-P(NIPMA-MAA) were evaluated with FTIR technique. Crystallinity and phase composition of Ag/Ni-P(NIPMA-MAA) were evaluated with X-ray diffraction (Bruker D8 Advance Eco) and morphology with a transmission electron microscope

(JEOLJEM-1230). The elements present in Ag/Ni-P(NIPMA-MAA) were identified with energy-dispersive spectroscopy (EDS). The stability of nanoparticles into microgel and catalytic performance results of Ag/Ni-P(NIPMA-MAA) were obtained with the help of UV-visible spectrophotometer (Shimadzu UV-3600) with temperature controlled. BI-200SM (Brookhaven Instrument Corp., US) was used hydrodynamic diameter (D_h) of microgels and hybrid microgels. The pH meter (PHS-3CU) was used to find the pH of the medium.

2.4 Catalytic activity of Ag/Ni-P(NIPMA-MAa)

Catalytic performance of Ag/Ni-P(NIPMA-MAa) was checked against reduction of (MOr), (MRe), (EBlT), and CRe dyes in the presence of reductant (NaBH$_4$) from aqueous medium. During the kinetic study, the effect of concentrations of reductant, dyes and catalyst was also studied. The degraded products were separated by physical separation method and characterized by ^{1}H NMR as shown in Fig. 1S.†

3 Results and discussion

3.1 Synthesis of P(NMA-MAa) and Ag/Ni-P(NMA-MAa)

The synthesis of P(NMA-MAa) and Ag/Ni-P(NMA-MAa) are shown in Fig. 1.[32] The P(NMA-MAa) microgels were synthesized by FRPPM. Then the mixture of Ag and Ni metal salts were encapsulated into the reaction mixture. The Ag$^+$ ions and Ni^{2+} ions came into the sieves of crosslinked polymeric network of P(NMA-MAa) from bulk region in slightly basic medium due to formation of dative bond.

In P(NMA-MAa) microgels, there are two functional groups in their structure which have the capacity to donate lone pair of electrons to transition metal ions (Ag$^+$ ions, Ni^{2+} ions). One of them is amide and other is carboxylic. In slightly basic medium, the carboxylic groups of P(NMA-MAa) microgels are present deprotonated form and microgels are present in swollen state due to electrostatic repulsion between deprotonated carboxylic groups and in this state, maximum metal ions are loaded into the microgels. Then these metal ions were reduced into respective atomic form by in situ reduced. These atoms start to coagulate to form a cluster of atoms which is controlled with the help of different functionalities present in structure of P(NMA-MAa) microgels.

3.2 Characterizations of P(NMA-MAa) and Ag/Ni-P(NMA-MAa)

The synthesized P(NMA-MAa) and Ag/Ni nanoparticles loaded P(NMA-MAa) were characterized with FTIR as shown in Fig. 2. The stretching band of –OH groups present in both P(NMA-MAa) and Ag/Ni-P(NMA-MAa) were appeared at 3346.03 cm^{-1}. The C–H stretching band of –CH$_3$ of MAa was appeared at 2970.44 cm^{-1}. The peak of carbonyl groups presents in of P(NMA-MAa) and Ag/Ni-P(NMA-MAa) appeared at 1631.01 cm^{-1}. The FTIR results showed that P(NMA-MAa) and Ag/Ni-P(NMA-MAa) have same functionalities and Ag/Ni nanoparticles do not effect on hierarchy of functional groups.[16]
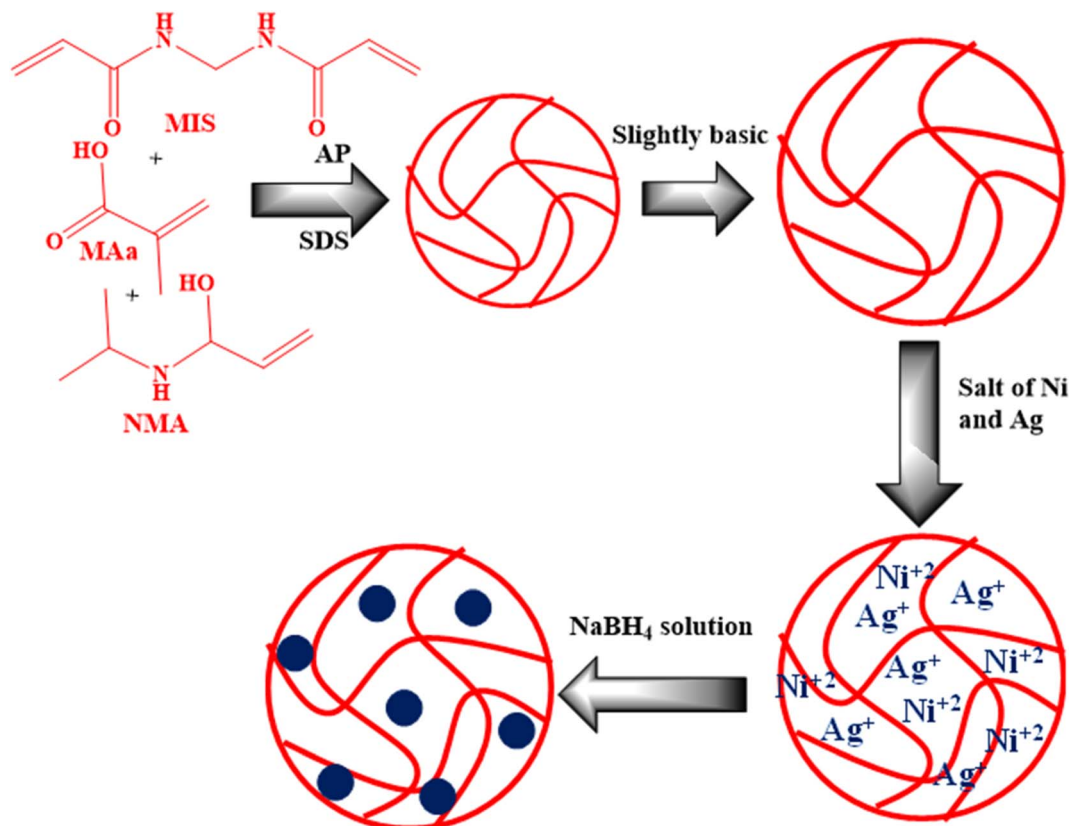
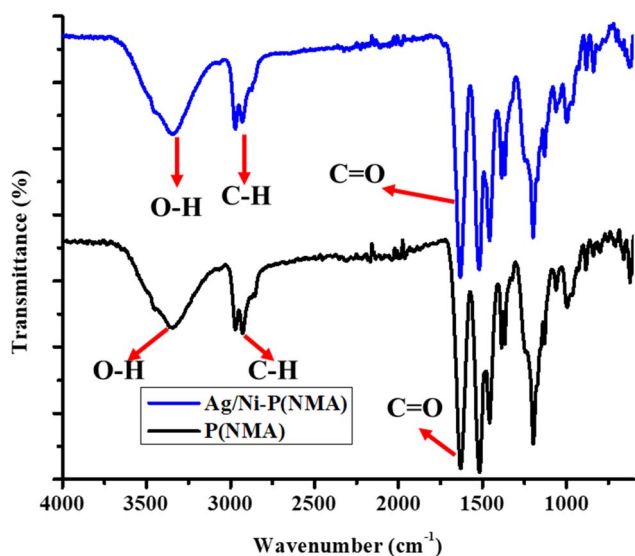Fig. 1   Pictorial diagram of synthesis of P(NMA-MAa) and Ag/Ni-P(NMA-MAa).

Fig. 2   FTIR spectra of synthesized P(NMA-MAa) and Ag/Ni-P(NMA-MAa).

The elements present in P(NMA-MAa) microgels and Ag/Ni-P(NMA-MAa) hybrid microgels were identified with the help of EDX as shown in Fig. 3(A and B). The elements present in P(NMA-MAa) are shown in Fig. 3(A) and element in Ag/Ni nanoparticles loaded into P(NMA-MAa) shown in Fig. 3(B).

The P(NMA-MAa) had only C, N and O elements in their structure while Ag/Ni nanoparticles loaded P(NMA-MAa) had Ag and Ni along with C, N, and O elements. These results confirmed that Ag and Ni elements were present in Ag/Ni nanoparticles loaded in P(NMA-MAa).

The degree of crystallinity of both P(NMA-MAa) and Ag/Ni-P(NMA-MAa) were found by XRD as shown in Fig. 2S.† The P(NMA-MAa) microgels were found in amorphous in nature but crystallinity was present in Ag/Ni-P(NMA-MAa) due to presence of Ag/Ni nanoparticles. Different peaks of Ag/Ni nanoparticles were appeared in the XRD spectra of both microgels and hybrid microgels. The appearance of different peaks in XRD spectra of hybrid microgels confirmed the presence of Ag/Ni nanoparticles in microgels.[33–36]

The endowment of Ag/Ni nanoparticles in P(NMA-MAa) microgels was confirmed by UV-visible spectroscopy as shown in Fig. 4. The diluted dispersions of P(NMA-MAa) and Ag/Ni-P(NMA-MAa) were run in a UV-visible spectrophotometer at room temperature (26 °C). No clear peak was observed in P(NMA-MAa) dispersion while a clear peak at 301 nm was observed during the running of Ag/Ni-P(NMA-MAa) dispersion. The peak was due to λ_{spr} of surface plasmon resonance of Ag/Ni nanoparticles present in P(NMA-MAa). The spectra confirmed the presence of Ag/Ni nanoparticles in P(NMA-MAa).[37]

The thermal stability of P(NMA-MAa) and Ag/Ni-P(NMA-MAa) were elucidated with TGA. Initially, the water molecules lost from both P(NMA-MAa) and Ag/Ni-P(NMA-MAa) at 100 °C.
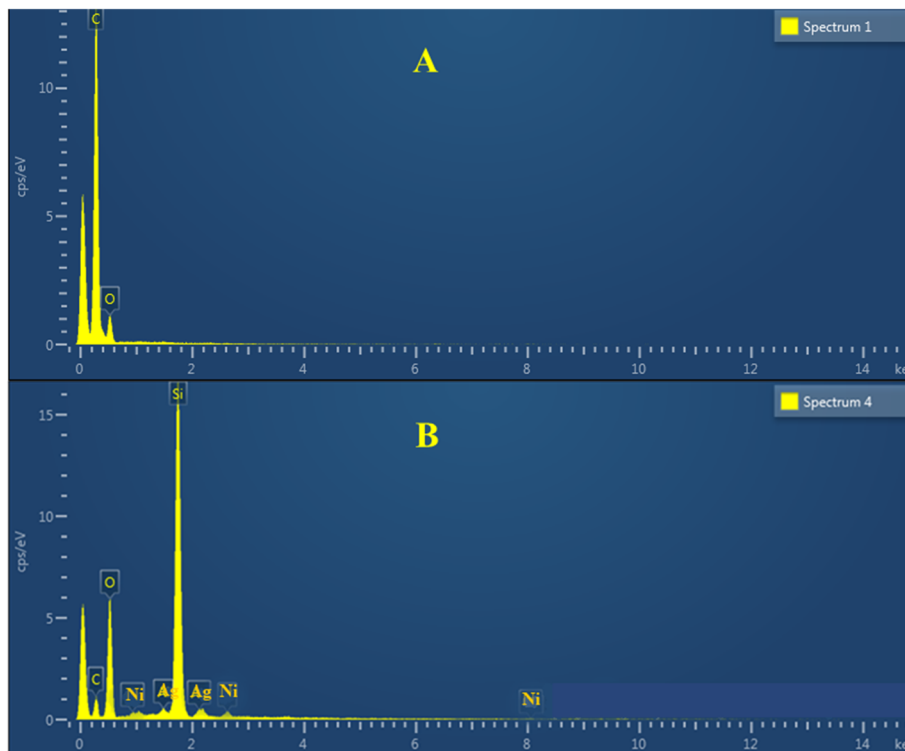
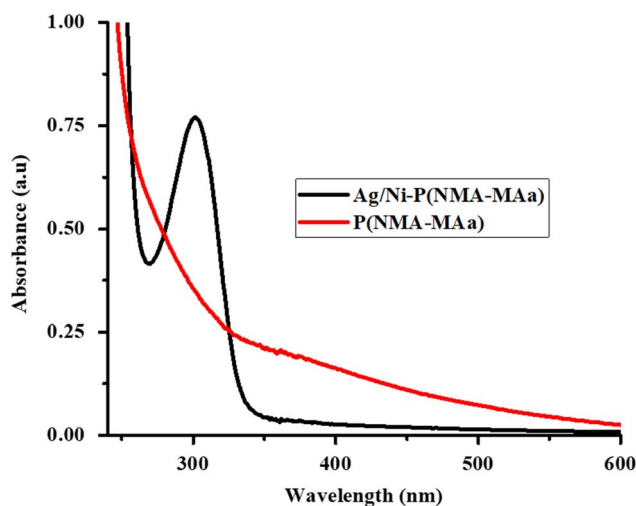**Fig. 3** EDX results of (A) P(NMA–MAa) and (B) Ag/Ni–P(NMA–MAa).

Fig. 4 UV-visible spectra of P(NMA–MAa) and Ag/Ni nanoparticles loaded in P(NMA–MAa) at 26 °C and pH = 5.5.

80% weight was lost from P(NMA–MAa) at 435 °C while Ag/Ni-P(NMA–MAa) lost at 425 °C. 5% of Ag/Ni nanoparticles were present in Ag/Ni-P(NMA–MAa) which was evaluated from Fig. 5(A). The size and size distribution of P(NMA–MAa) and Ag/Ni-P(NMA–MAa) were examined with DLS as shown in Fig. 5(B). The hydrodynamic diameter (D_h) of P(NMA–MAa) was found to be greater than Ag/Ni-P(NMA–MAa) due to occupation of some cavity of crosslinked polymer by Ag/Ni nanoparticles. Therefore, small number of water molecules come into the sieves and hence, small swelling occurred as compared to P(NMA–MAa).

The sizes and morphologies of P(NMA–MAa) and Ag/Ni nanoparticles present in P(NMA–MAa) were identified with the help of STEM results. The morphologies of P(NMA–MAa) and Ag/Ni nanoparticle present in P(NMA–MAa) were spherical as shown in Fig. 3S.† The mean diameter of Ag/Ni nanoparticles was found 44.06 ± 11.64 and 268.88 ± 91.34 of P(NMA–MAa) microgels. These results confirmed that Ag/Ni nanoparticles were present in P(NMA–MAa) and both had spherical morphology. The XRD and STEM results of hybrid microgels indicated that Ag/Ni nanoparticles were present in alloy form.[38–40] The size of P(NMA–MAa) and Ag/Ni-P(NMA–MAa) were found smaller than in DSL results. The sample in DLS were run in aqueous medium. So, D_h of both increases due to swelling behavior but STEM results were performed in the absence of water. Therefore, the diameters of P(NMA–MAa) and Ag/Ni-P(NMA–MAa) in STEM results were found to be smaller than DLS results.

To check the stability of Ag/Ni nanoparticles present in P(NMA–MAa) microgels. The spectra of dispersion of Ag/Ni nanoparticles loaded P(NMA–MAa) were obtained after running the dispersion medium with different intervals as shown in Fig. 6. No significant decline was observed in λ_{spr} value of Ag/Ni nanoparticles loaded P(NMA–MAa). These results of Ag/Ni nanoparticles loaded P(NMA–MAa) microgels indicate that Ag/Ni nanoparticles are stabilized with the help of P(NMA–MAa) microgels for a long time.[22]

The effect of stimuli responsive behavior of microgels on λ_{spr} of Ag/Ni nanoparticles was also studied. The effect of pH of the medium on shifting of λ_{spr} of Ag/Ni nanoparticles by swelling
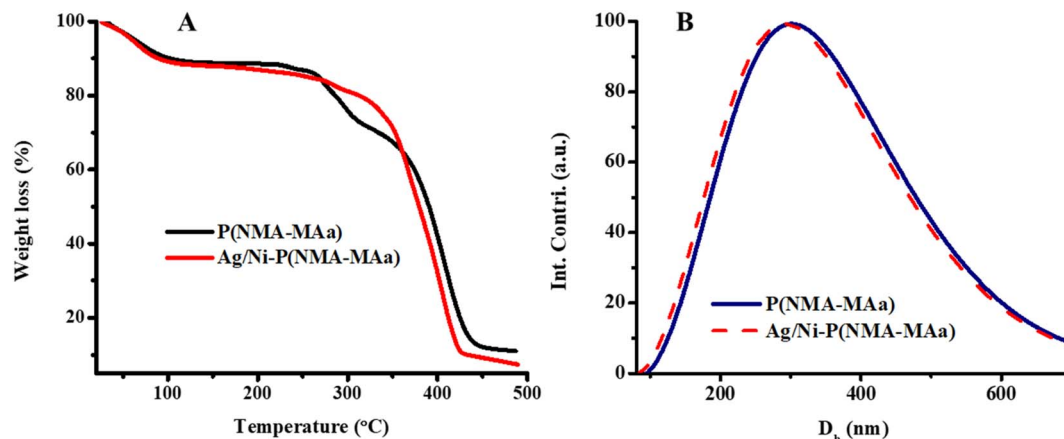
Fig. 5 (A) TGA spectra of P(NMA-MAa) and Ag/Ni nanoparticles loaded in P(NMA-MAa) and (B) DLS results at 26 °C and pH = 5.5.
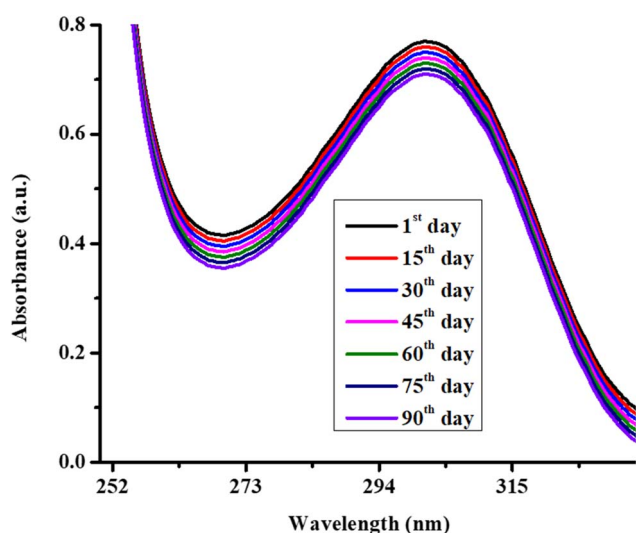

Fig. 6 UV-visible spectra of Ag/Ni nanoparticles loaded P(NMA-MAa) microgels at room temperature (26 °C) and pH = 6.5.

P(NMA-MAa) microgels were present in deprotonated forms (–COO$^-$). Due to presence of same charge on carboxylate ions, electrostatic repulsion occurs and P(NMA-MAa) microgels were present in swelling state and large space was present for oscillation of surface electrons. So, the speed of oscillation was decreased and hence, low energy (high wavelength) was required for coupling with oscillating surface electron of Ag/Ni nanoparticles. Therefore, λ_{spr} of Ag/Ni nanoparticles loaded in P(NMA-MAa) microgels were shifted to lower energy or higher wavelength at increasing the pH of the medium. The aggregation of Ag/Ni nanoparticles into P(NMA-MAa) microgels by escaping the nanoparticles from one sieve to other may be another reason of this shifting. One of our group has also reported similar results.[41] Here, further investigation is required for complete information about the actual reason of such behavior.

Similarly, temperature effect of λ_{spr} value of Ag/Ni nanoparticles in P(NMA-MAa) microgels was also investigated as show in Fig. 7(B) at pH = 5.5. The effect of temperature was indicated that Ag/Ni nanoparticles were stable for various temperature range (20–80 °C). The λ_{spr} value of Ag/Ni nanoparticles were shifted from 300 nm to 316 nm as increasing the temperature from 20 °C to 80 °C. This red shifting was occurred due to change in refractive index and inter particles distance. As increasing the temperature from 20 °C to 40 °C, no significant red shift was observed while increasing the temperature firm 40 °C to 80 °C, a rapid red shifting was observed. The volume phase transition temperature (VPTT) of P(NMA-MAa) is almost 46 °C. Therefore, initially by increasing the temperature (T < 46 °C), the deswelling behavior of P(NMA-MAa) was slightly but became more prominent after temperature (46 °C). Due to deswelling behavior of P(NMA-MAa), the refractive index of Ag/Ni nanoparticles loaded in P(NMA-MAa) was increased and hence, red shifting was occurred in λ_{spr}.[41]

3.3 Use of Ag/Ni-P(NMA-MAa) as catalyst

The synthesized Ag/Ni nanoparticles loaded P(NMA-MAa) microgels were used as catalyst for degradation of MOr, MRe, CRe and EBlT from aqueous medium. The degradation of MOr

and deswelling behavior of microgels is shown in Fig. 7(A) and temperature in Fig. 7(B). The Fig. 7(A) shows that the Ag/Ni nanoparticles loaded into P(NMA-MAa) are stable at various pH of the medium. At low pH (pH > pK_a of MAa), the surface plasmon resonance value was obtained at low wavelength while red shifting in λ_{spr} value was observed as increasing the pH of the medium. This red shifting behavior was due to stimuli responsive behavior of P(NMA-MAa). The λ_{spr} value was shifted from 298 nm to 310 nm as increasing the pH of the medium from 1 to 11. At low pH, the carboxylic groups, present in the structure of P(NMA-MAa), were present in protonated form and P(NMA-MAa) microgels were present in deswelling state. In this form, small region was present for loaded Ag/Ni nanoparticles into the sieves of P(NMA-MAa). At this condition, the surface electrons of Ag/Ni NPs were forced to live in on a small surface area. In this condition, the surface electrons were oscillated with high speed and hence high energy (low wavelength) was required for resonance. But at high pH, the carboxylic groups of
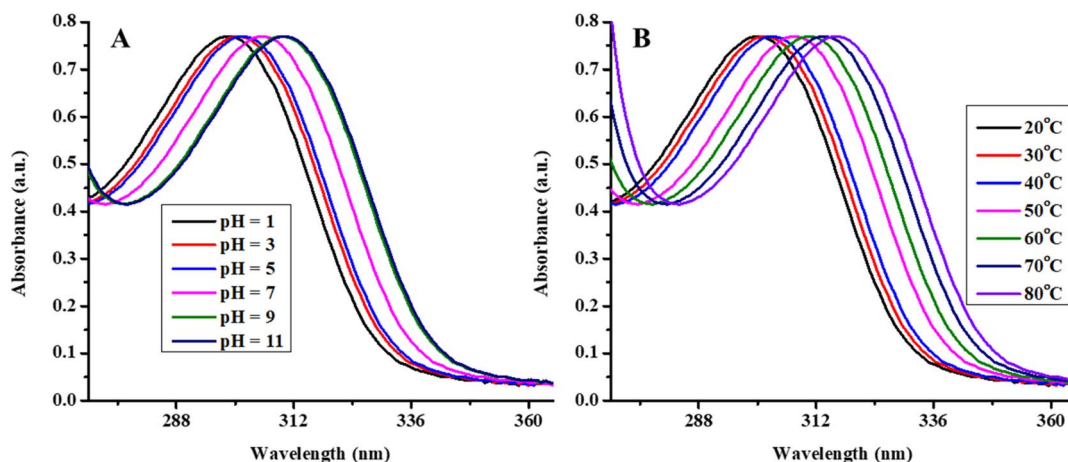
Fig. 7 UV-visible spectra of Ag/Ni-P(NMA-MAa) at (A) various pH (1–11) and (B) various temperature (20–80 °C).

was used as model for catalytic degradation reaction. For this purpose, solutions of MOr, NaBH$_4$ (reductant) and Ag/Ni-P(NMA-MAa) were mixed in a cuvette and run the spectra in a UV-visible spectrophotometer. The obtained graph is as shown in Fig. 8(A). The MOr was degraded within 8 min in the presence of Ag/Ni-P(NMA-MAa) (catalyst) and NaBH$_4$ (reductant). Then, some controlled experiments were performed to find the true catalyst. For this purpose, the solutions of MOr, NaBH$_4$ and P(NMA-MAa) were mixed into a cuvette and run the reaction mixture. In the λ_{max} (460 nm) value, no decline was
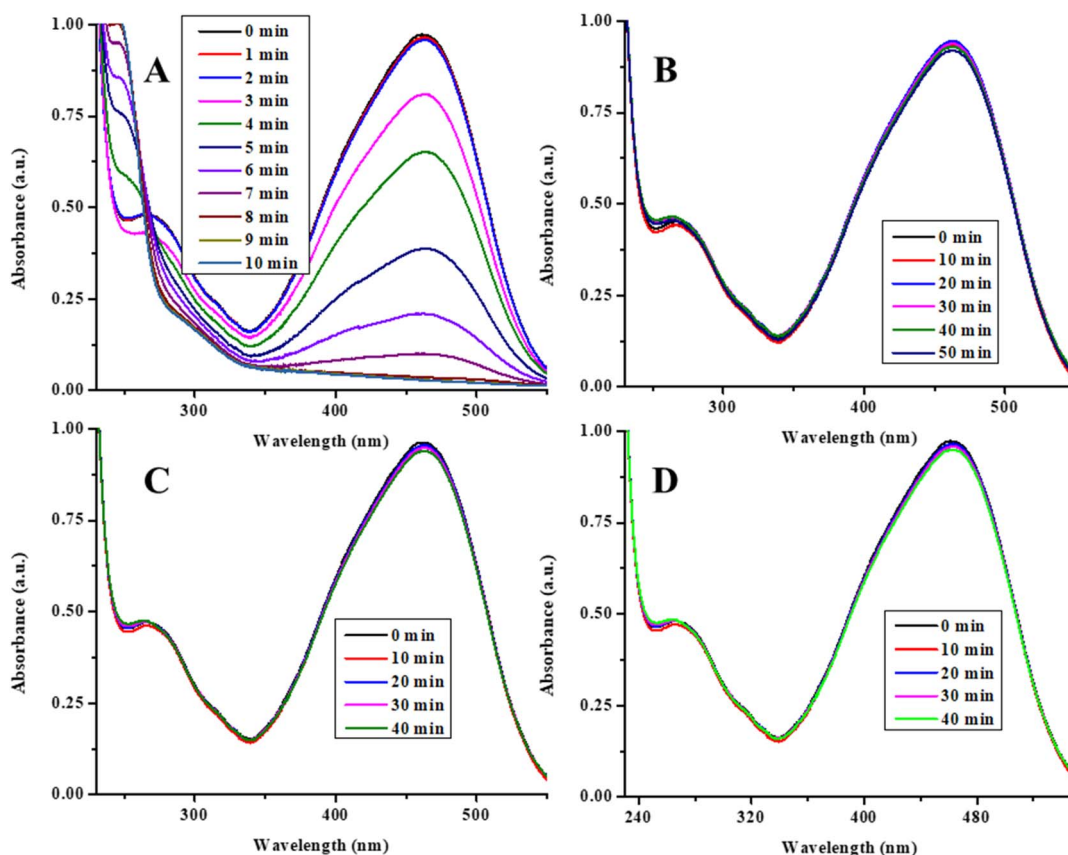

Fig. 8 Controlled experiment of catalytic degradation of MOr at (A) NaBH$_4$, MOr, and Ag/Ni-P(NMA-MAa) [conditions: [MOr] = 0.080 mM, [NaBH$_4$] = 9.65 mM, Ag/Ni-P(NMA-MAa) = 85.71 μg mL^{-1}], (B) MOr, NaBH$_4$ and P(NMA-MAa) [conditions: [MOr] = 0.080 mM, P(NMA-MAa) = 9.65 μg mL^{-1}, [NaBH$_4$] = 9.65 mM] (C) MOr and NaBH$_4$ [conditions: [MOr] = 0.080 mM, [NaBH$_4$] = 9.65 mM, without addition of P(NMA-MAa) and Ag/Ni-P(NMA-MAa)], (D) MOr and Ag/Ni-P(NM) [conditions: [MOr] = 0.080 mM, Ag/Ni-P(NMA-MAa) = 85.71 μg mL^{-1}, in the absence of NaBH$_4$].

observed till 50 min as shown in Fig. 8(B). Then, only NaBH$_4$ solution was added into the MOr solution and run this mixture. No degradation was observed till 40 min as shown in Fig. 8(C). In the last, only Ag/Ni-P(NMA-MAa) was put into the MOr solution and run. The results showed that no degradation occurred as shown in Fig. 8(D). All these results indicated that Ag/Ni nanoparticles were true catalyst, and their catalytic performance required the presence of reductant (NaBH$_4$) to degrade organic dyes. Ag/Ni nanoparticles provide the surface for catalytic degradation of dyes.[16]

The Ag/Ni nanoparticles loaded in P(NMA-MAa) microgels are stabilized for long time with the help of P(NMA-MAa) microgels. This system has excellent catalytic activity for degradation of organic dyes. That is why, herein, Ag/Ni nanoparticles loaded in P(NMA-MAa) were synthesized and used for degradation of dyes as shown in Fig. 8(A) (catalytic degradation of MOr).

To study the effect of concentration of Ag/Ni nanoparticles loaded into P(NMA-MAa) microgels on kinetic study was observed by increasing the concentration of Ag/Ni-P(NMA-MAa) from 54.74 μg mL^{-1} to 118.22 μg mL^{-1} in the reaction mixture while concentrations of NaBH$_4$ and MOr was keeping constant at 9.65 mM and 0.080 mM respectively at pH = 5.56 and temperature 26 °C. The ln(A_0/A_t) vs. time (T) graph was plotted to study the kinetics as shown in Fig. 9(A). The initial time, in which degradation of MOr was not observed, is called induction time (T_i). After induction time, MOr was started to degrade and this time during which dye starts to degrade to complete degradation is called reaction time (T_r). This is the time which is used for study of kinetic of catalytic degradation of dyes. After this time, no further degradation of dye occurs. This time is called completion time (T_c). The k_0 value was calculated by applying linear equation ln(A_t/A_0) = $k_0 T_r$ + c. The k_0 value is equal to the slope of linear equation. The value of T_i decreased with increasing the concentration of Ag/Ni-P(NMA-MAa) as shown in Fig. 9(A). The value of k_0 was decreased as increasing the amount of Ag/Ni-P(NMA-MAa). The k_0 vs. time graph was also plotted to study the relationship of time with slope of

catalytic degradation. The k_0 value increased linearly with time as shown in Fig. 9(B). The results showed that catalytic degradation rate of MOr was increased with increasing the dose of Ag/Ni-P(MNA-MAa). This behavior is due to increasing the active sites of catalyst with increasing the amount of Ag/Ni-P(NMA-MAa). Similar result was obtained in our previous article.[29]

The effect of concentration of MOr on catalytic degradation rate was also studied. During this study, the range of concentration of MOr was 0.070–0.100 mM while the other parameters were kept constant (temperature = 26 °C, pH = 5.56, Ag/Ni-P(NMA-MAa) = 85.71 μg mL^{-1} and NaBH$_4$ = 9.65 mM). The T_i and T_c values were decreased first and then increased as shown in Fig. 10(A). The ln(A_t/A_0) vs. T dependent graph of catalytic degradation reaction of MOr was shown in Fig. 10(A). The apparent rate constant (k_0) catalytic degradation was obtained by applying pseudo first order kinetic equation. For calculation of k_0, only reaction time was used. The k_0 vs. T dependent graph was shown in Fig. 10(B).

This graph showed that the value of k_0 increased as increasing the concentration of MOr from 0.070 mM to 0.085 mM while k_0 value decreased for further increasing the concentration from 0.085 mM to 0.100 mM. Initially, as increasing the concentration of MOr, more substrate reaches on the surface of Ag/Ni-P(NMA-MAa) and degradation rate increased but after further increment in concentration of MOr cased the increasing the number of collision and hence, less chance to the substrate to reach on the surface of Ag/Ni nanoparticles loaded P(NMA-MAa). So, the value of k_0 was started to decrease after certain concentration.[42]

Similarly, the effect of concentration of NaBH$_4$ on catalytic degradation rate of MOr was also studied. The T_i and T_c values were decreased initially and then increased again as shown in Table 1. The ln(A_t/A_0) vs. T dependent graph was shown in Fig. 11(A) and k_0 vs. concentration of NaBH$_4$ dependent in Fig. 11(B). The value of k_0 increased from 7.52 mM to 10.33 mM of concentration of NaBH$_4$ and then decreased on further increasing the concentration of NaBH$_4$ from 10.33 mM to 12.98 mM as shown in Fig. 11(B). Initially, the value of k_0
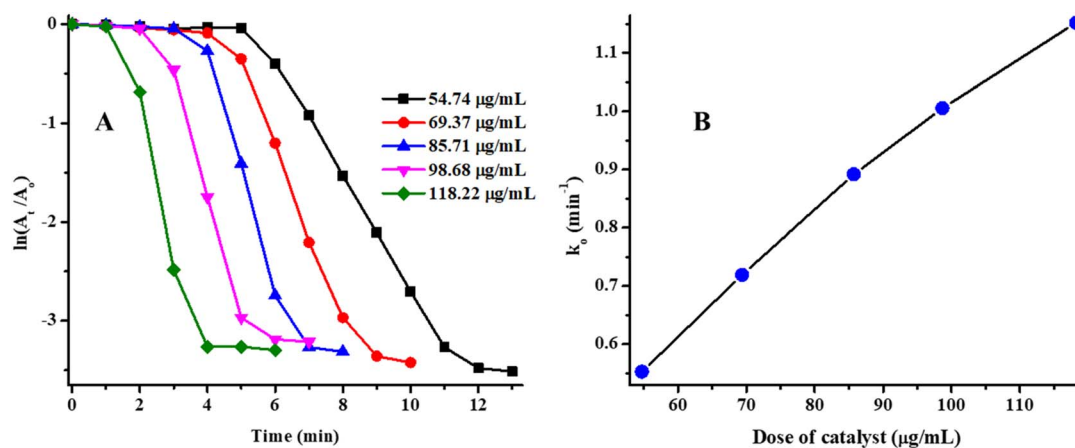

Fig. 9 Degradation of MOr dye (A) time vs. ln(A_t/A_0) plot under various concentrations of Ag/Ni-P(NMA-MAa) [conditions: NaBH$_4$ = 9.65 mM, pH = 5.56, concentration of MeOr = 0.080 mM, Ag/Ni-P(NMA-MAa) = (54.74–118.22) μg mL^{-1}] and (B) catalytic dose vs. k_0 at 26 °C.
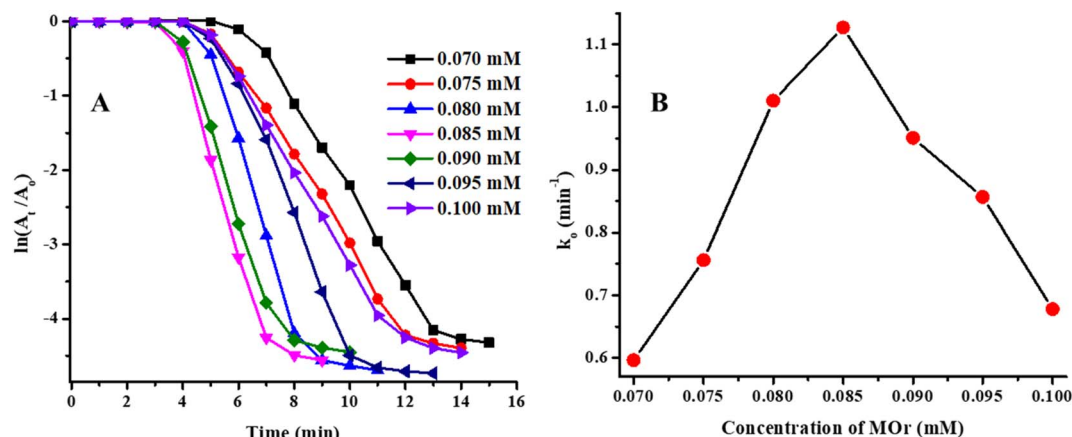
Fig. 10 Kinetics of catalytic degradation of MOr at 26 °C (A) $\ln(A_t/A_0)$ vs. T function for degradation of MOr (0.070–0.100 mM) in the presence of NaBH$_4$ (9.65 mM) and Ag/Ni-P(NMA-MAa) (85.71 μg mL^{-1}), (B) the k_0 vs. MOr concentration dependent graph.

increased due to rapidly reach of NaBH$_4$ on the surface of Ag/Ni nanoparticles through crosslinked network from bulk region but this behavior was possible only for certain concentration above which the concentration of NaBH$_4$ occupied more active sites of catalyst and less possibility for substrate (MOr) to reach on catalytic surface and hence, the value of k_0 were started to decrease.[22]

The comparison study of this system along with other bimetallic nanoparticles loaded in smart microgels are given in Table 2. Mostly, the bimetallic nanoparticles loaded smart microgels reported in literature have low catalytic activity than our system. The value of k_0 for catalytic reductive reaction of Ag/Ni-P(NMA-MAa) was better than previously reported similar systems.

3.4 Proposed catalytic degradation mechanism

The data of kinetic study was discussed in Section 3.3. This data revealed that the catalytic degradation process of MOr in the presence of Ag/Ni nanoparticles loaded in P(NMA-MAa)

microgels and reductant (NaBH$_4$) followed "Langmuir–Hinshelwood mechanism". In this mechanism, both reactant species (MOr and hydrogen produced from NaBH$_4$) are come through crosslinked network of polymer to the surface of Ag/Ni nanoparticles from aqueous medium and adsorbed on the surface of Ag/Ni nanoparticles. The reactants are then converted into degraded product and then desorbed from the surface of nanoparticles. The proposed mechanism of catalytic degradation of MOr in the presence of Ag/Ni-P(NMA-MAa) and NaBH$_4$ is shown in Fig. 12. In first step, NaBH$_4$ is reacted with water to produce NaB(OH)$_4$ and hydrogen molecules. These molecules diffuse to the surface of nanoparticles. The nitrogen atoms of azo group have lone pair. The nitrogen atom of azo group gains a proton from water molecule and resonance occurs to form (a). Then hydride attacks on electron deficient nitrogen atom of (a) to form (b). In the next step, nitrogen atom again gains a proton from water to form (c) and amine aryl compound. At the same time, hydride attacks on electron deficient nitrogen to form

Table 1 The values of concentrations of MOr, NaBH$_4$ and Ag/Ni-P(NMA-MAa), k_0, pH, T_i, T_c and half-life period

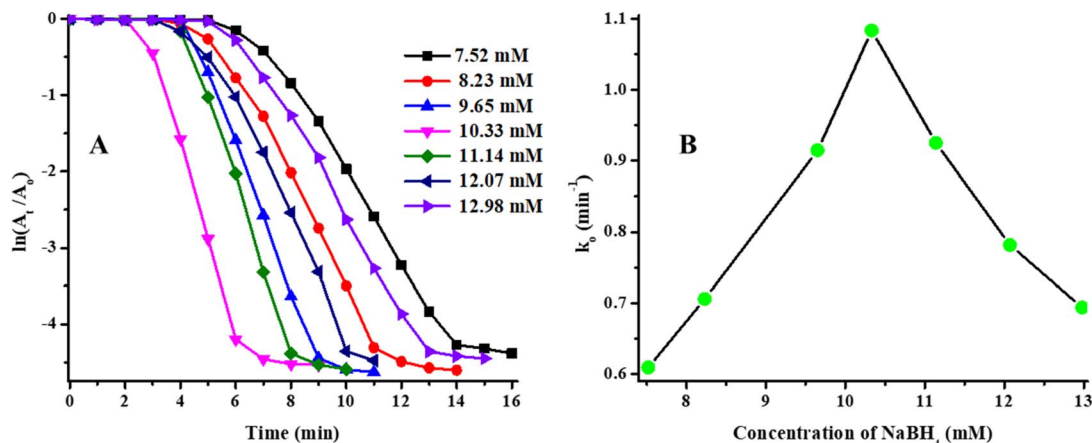| Reaction conditions	pH	MOr (mM)	NaBH$_4$ (mM)	Catalyst (μg mL^{-1})	T_i (min)	T_c (min)	k_0 (min^{-1})	$t_{1/2}$ (min)
NaBH$_4$	5.56	0.08	7.52	85.71	5	14	0.609	1.642
	5.56	0.08	8.23	85.71	4	11	0.706	1.416
	5.56	0.08	9.65	85.71	4	9	0.915	1.093
	5.56	0.08	10.33	85.71	2	6	1.083	0.923
	5.56	0.08	11.14	85.71	3	8	0.925	1.081
	5.56	0.08	12.07	85.71	3	10	0.782	1.279
	5.56	0.08	12.98	85.71	5	12	0.694	1.441
Catalyst	5.56	0.08	9.65	54.74	5	11	0.553	1.808
	5.56	0.08	9.65	69.37	4	9	0.72	1.389
	5.56	0.08	9.65	85.71	3	7	0.892	1.121
	5.56	0.08	9.65	98.68	2	5	1.006	0.994
	5.56	0.08	9.65	118.22	1	4	1.152	0.868
MeOr	5.56	0.070	9.65	85.71	6	13	0.596	1.678
	5.56	0.075	9.65	85.71	4	12	0.756	1.323
	5.56	0.080	9.65	85.71	4	9	1.011	0.989
	5.56	0.085	9.65	85.71	3	7	1.127	0.887
	5.56	0.090	9.65	85.71	3	8	0.951	1.052
	5.56	0.095	9.65	85.71	4	10	0.857	1.167
	5.56	0.100	9.65	85.71	4	12	0.678	1.475

Fig. 11 Effect of concentration of NaBH$_4$ on catalytic degradation of MOr at 26 °C (A) ln(A_t/A_0) vs. T function for degradation of MOr (0.080 mM) in the presence of NaBH$_4$ (7.52–12.98 mM) and Ag/Ni-P(NMA-MAa) (85.71 µg mL^{-1}), (B) the k_0 vs. NaBH$_4$ concentration dependent graph.

Table 2 Comparison of Ag/Ni-P(NMA-MAa) with other similar systems

Catalyst	Abbreviations	Substrate	Apparent rate constant (k_0) (min^{-1})	Reference
Ag/Co nanoparticles loaded into poly(N-isopropyl methacrylamide)	Ag/Co-P(NMA)	MOr	0.481	43
Ag/Au nanoparticles loaded in poly(N-isopropyl acrylamide-co-3-methacryloxypropyltri methoxysilane)	Ag/Au-P(NA-MPS)	4NPe	0.174 min^{-1}	27
Ag/Au nanoparticles in poly(N-isopropyl acrylamide co acrylic acid)	Ag/Au-P(NA-AA)	4NPe	0.215	26
Polystyrene surrounded by Ag/Pd nanoparticles loaded in poly(N-isopropyl acrylamide)	Ag/Pd-P(ST@NA)		0.120 min^{-1}	44
Ag/Ni nanoparticles in poly(N-isopropyl methacrylamide-methacrylic acid)	Ag/Ni-P(NMA-MAa)	MOr	0.925 min^{-1}	This work
		CRe	0.486 min^{-1}	This work
		EBlT	0.540 min^{-1}	This work
		MRe	0.525 min^{-1}	This work

product. The OH$^-$ ions, produced after donation of proton to MOr, combines with boron to form B(OH)$_4$$^{-1}$ ions. After conversion of MOr into product, detach from the surface and diffuse towards the aqueous medium from the surface of Ag/Ni nanoparticles through cross linked network of P(NMA-MAa).[16,26,45–48] The degraded product was characterized by ^{1}H NMR which supported this mechanism as shown in Fig. 1S.†

3.5 Catalytic degradation of other dyes

The EBlT, CRe and MRe were also catalytically degraded in the presence of Ag/Ni nanoparticles loaded in P(NMA-MAa) microgels and reductant (NaBH$_4$) from aqueous medium. The catalytic degradation reaction data was shown in Fig. 4S(A–C).† The Ag/Ni nanoparticles showed good result for catalytic degradation of organic dyes from aqueous medium.

3.6 Catalytic reduction recycling process

The catalytic activity of Ag/Ni nanoparticles loaded P(NMA-MAa) microgels was also studied after regaining by centrifugation

after complete degradation of dye. For this purpose, MOr dye was used as model of catalytic degradation reaction.

The Ag/Ni-P(NMA-MAa) was recovered after complete degradation of MOr and then again used as catalyst to degrade further molecules of MOr present in new solution of MOr dye. The k_0 values were calculated for each catalytic degradation cycle. The eqn (1) was used to calculate percentage catalytic activity of Ag/Ni-P(NMA-MAa).

$$\text{Percentage catalytic activity}(\%) = \frac{k_0(n^{\text{th}}\text{ cycle})}{k_0(1^{\text{st}}\text{ cycle})} \times 100 \quad (1)$$

The percentage catalytic activity of Ag/Ni-P(NMA-MAa) was shown in Fig. 13. The catalytic activity of Ag/Ni nanoparticles loaded P(NMA-MAa) microgels were almost same after recycling. The catalytic activity was obtained 92 percent after five cycles as shown in Fig. 13. Slight decline in catalytic activity of Ag/Ni-P(NMA-MAa) hybrid microgels may be due loss of catalytic contents during decantation and centrifugation steps of recycling process.
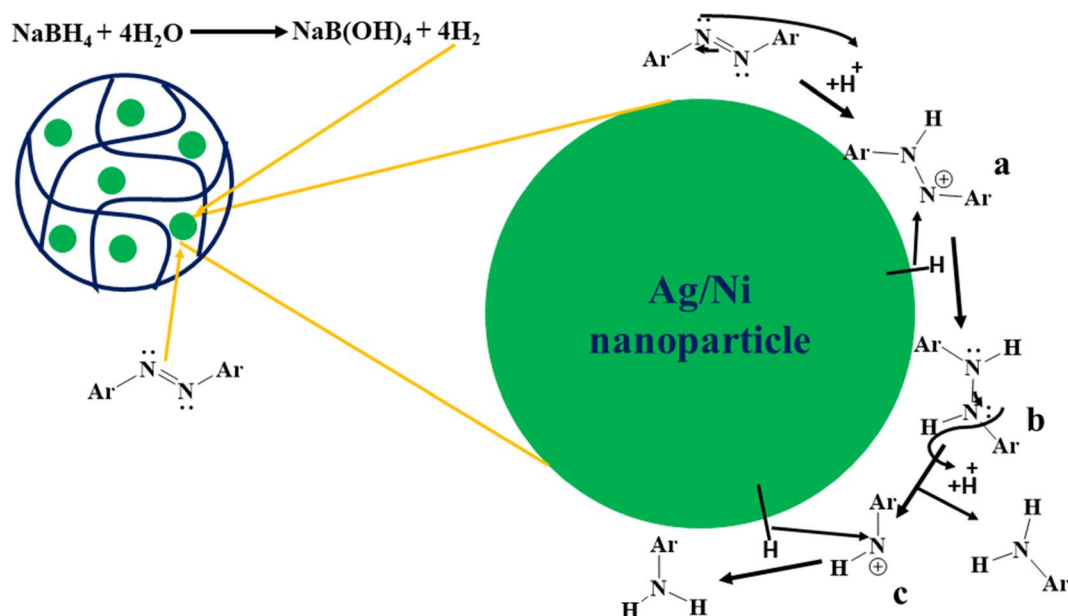
Fig. 12 Proposed mechanism of catalytic degradation reaction of MOr in the presence of Ag/Ni-P(NMA-MAa) and NaBH$_4$.
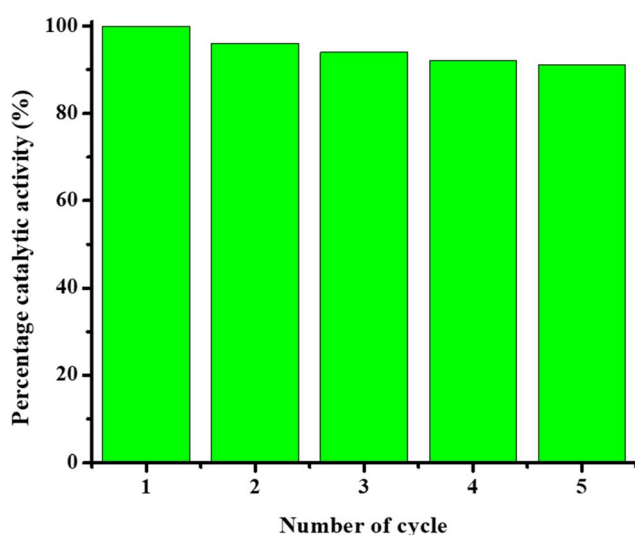

Fig. 13 The catalytic activity percentage of Ag/Ni-P(NMA-MAa) system used for catalytic degradation of MOr [conditions: Ag/Ni-P(NMA-MAa) = 85.71 μg mL^{-1}, concentration of MOr = 0.080 mM, NaBH$_4$ = 9.65 mM].

4 Conclusion

The P(NMA-MAa) microgel particles were synthesized by radical precipitation polymerization method and then Ag/Ni nanoparticles into crosslinked network of P(NMA-MAa) by *in situ* reduction method. The bimetallic (Ag/Ni) nanoparticles loaded P(NMA-MAa) microgel system showed swelling and deswelling behavior by external stimuli. The P(NMA-MAa) system exhibited the excellent stabilizing property towards the bimetallic nanoparticles. The Ag/Ni-P(NMA-MAa) hybrid microgels were found an excellent catalyst for degradation of organic dyes in aqueous

medium. The catalytic degradation reaction followed "Langmuir–Hinshelwood mechanism". Under mild conditions, Ag/Ni-P(NMA-MAa) system can be used for catalytic degradation of all type of organic dyes from aqueous medium. The Ag/Ni-P(NMA-MAa) system showed 92 percent catalytic activity even after five cycles.

Data availability

The data that support the findings of this study are available from the corresponding author upon reasonable request.

Conflicts of interest

There are no conflicts to declare.

Acknowledgements

References

1 S. Benkhaya, S. M'rabet and A. El Harfi, Classifications, properties, recent synthesis and applications of azo dyes, *Heliyon*, 2020, **6**, e03271, DOI: **10.1016/j.heliyon.2020.e03271**.
2 M. Moustakas, The Role of Metal Ions in Biology, Biochemistry and Medicine, *Materials*, 2021, **14**, 549, DOI: **10.3390/ma14030549**.
3 H. Tokiwa, Y. Ohnishi and H. S. Rosenkranz, Mutagenicity and Carcinogenicity of Nitroarenes and Their Sources in the Environment, *Crit. Rev. Toxicol.*, 1986, **17**, 23–58, DOI: **10.3109/10408448609037070**.

4 M. A. Hassaan and A. El Nemr, Pesticides pollution: Classifications, human health impact, extraction and treatment techniques, *Egypt. J. Aquat. Res.*, 2020, **46**, 207–220, DOI: 10.1016/j.ejar.2020.08.007.

5 F. I. Vacchi, J. A. de S. Vendemiatti, B. F. da Silva, M. V. B. Zanoni and G. de A. Umbuzeiro, Quantifying the contribution of dyes to the mutagenicity of waters under the influence of textile activities, *Sci. Total Environ.*, 2017, **601–602**, 230–236, DOI: 10.1016/j.scitotenv.2017.05.103.

6 H. A. Shindy, Fundamentals in the chemistry of cyanine dyes: a review, *Dyes Pigm.*, 2017, **145**, 505–513, DOI: 10.1016/j.dyepig.2017.06.029.

7 G. Shabir, M. Arif, A. Saeed and G. Hussain, Synthesis and Optical Study of Sensitive and Selective Calix[4] Based Cu^{2+} Ion Detection Probes, *Russ. J. Gen. Chem.*, 2019, **89**, 813–818, DOI: 10.1134/S1070363219040285.

8 L.-H. Ahlström, C. Sparr Eskilsson and E. Björklund, Determination of banned azo dyes in consumer goods, *TrAC, Trends Anal. Chem.*, 2005, **24**, 49–56, DOI: 10.1016/j.trac.2004.09.004.

9 W. Liu, C. Fan, Z. Zong, N. Li, K. Ma, B. Zhu, X. Zhang and Y. Fan, Two Co(ıı)-based metal organic frameworks for highly efficient removal of azo dyes from aqueous environment: synthesis, selective adsorption and adsorption mechanism, *Colloids Surf. A Physicochem.*, 2020, **603**, 125236, DOI: 10.1016/j.colsurfa.2020.125236.

10 O. Gungor, A. Yilmaz, S. Memon and M. Yilmaz, Evaluation of the performance of calix[8]arene derivatives as liquid phase extraction material for the removal of azo dyes, *J. Hazard. Mater.*, 2008, **158**, 202–207, DOI: 10.1016/j.jhazmat.2008.01.060.

11 E. Yilmaz, S. Memon and M. Yilmaz, Removal of direct azo dyes and aromatic amines from aqueous solutions using two β-cyclodextrin-based polymers, *J. Hazard. Mater.*, 2010, **174**, 592–597, DOI: 10.1016/j.jhazmat.2009.09.093.

12 L. R. Shultz, L. Hu, K. Preradovic, M. J. Beazley, X. Feng and T. Jurca, A Broader-scope Analysis of the Catalytic Reduction of Nitrophenols and Azo Dyes with Noble Metal Nanoparticles, *ChemCatChem*, 2019, **11**, 2590–2595, DOI: 10.1002/CCTC.201900260.

13 M. Arif, M. Shahid, A. Irfan, X. Wang, H. Noor, Z. H. Farooqi and R. Begum, Catalytic degradation of organic dyes using Au-poly(styrene@N-isopropylmethacrylamide) hybrid microgels, *Inorg. Chem. Commun.*, 2022, **144**, 109870, DOI: 10.1016/j.inoche.2022.109870.

14 M. Arif, M. Shahid, A. Irfan, J. Nisar, X. Wang, N. Batool, M. Ali, Z. H. Farooqi and R. Begum, Extraction of copper ions from aqueous medium by microgel particles for *in situ* fabrication of copper nanoparticles to degrade toxic dyes, *Z. Phys. Chem.*, 2022, **236**(9), 1219–1241, DOI: 10.1515/zpch-2022-0038.

15 M. Arif, Complete life of cobalt nanoparticles loaded into cross-linked organic polymers: a review, *RSC Adv.*, 2022, **12**, 15447–15460, DOI: 10.1039/D2RA01058E.

16 M. Arif, M. Shahid, A. Irfan, J. Nisar, W. Wu, Z. H. Farooqi and R. Begum, Polymer microgels for the stabilization of gold nanoparticles and their application in the catalytic reduction of nitroarenes in aqueous media, *RSC Adv.*, 2022, **12**, 5105–5117, DOI: 10.1039/D1RA09380K.

17 M. Arif, Z. H. Farooqi, A. Irfan and R. Begum, Gold nanoparticles and polymer microgels: last five years of their happy and successful marriage, *J. Mol. Liq.*, 2021, **336**, 116270, DOI: 10.1016/j.molliq.2021.116270.

18 M. Shahid, Z. H. Farooqi, R. Begum, M. Arif, W. Wu and A. Irfan, Hybrid Microgels for Catalytic and Photocatalytic Removal of Nitroarenes and Organic Dyes From Aqueous Medium: A Review, *Crit. Rev. Anal. Chem.*, 2020, **50**, 513–537, DOI: 10.1080/10408347.2019.1663148.

19 T. Song, F. Gao, S. Guo, Y. Zhang, S. Li, H. You and Y. Du, A review of the role and mechanism of surfactants in the morphology control of metal nanoparticles, *Nanoscale*, 2021, **13**, 3895–3910, DOI: 10.1039/D0NR07339C.

20 R. B. Grubbs, Roles of Polymer Ligands in Nanoparticle Stabilization, *Polym. Rev.*, 2007, **47**, 197–215, DOI: 10.1080/15583720701271245.

21 K. Yamamoto, T. Imaoka, M. Tanabe and T. Kambe, New Horizon of Nanoparticle and Cluster Catalysis with Dendrimers, *Chem. Rev.*, 2020, **120**, 1397–1437, DOI: 10.1021/acs.chemrev.9b00188.

22 M. Shahid, Z. H. Farooqi, R. Begum, M. Arif, M. Azam, A. Irfan and U. Farooq, Multi-functional organic–inorganic hydrogel microspheres as efficient catalytic system for reduction of toxic dyes in aqueous medium, *Z. fur Phys. Chem.*, 2022, **236**, 87–105, DOI: 10.1515/zpch-2020-1739.

23 M. Arif, Journal of Environmental Chemical Engineering Extraction of iron(ııı) ions by core–shell microgel for *in situ* formation of iron nanoparticles to reduce harmful pollutants from water, *J. Environ. Chem. Eng.*, 2023, **11**, 109270, DOI: 10.1016/j.jece.2023.109270.

24 M. Shahid, Z. H. Farooqi, R. Begum, M. Arif, A. Irfan and M. Azam, Extraction of cobalt ions from aqueous solution by microgels for *in situ* fabrication of cobalt nanoparticles to degrade toxic dyes: a two fold-environmental application, *Chem. Phys. Lett.*, 2020, **754**, 137645, DOI: 10.1016/j.cplett.2020.137645.

25 R. Begum, Z. H. Farooqi, K. Naseem, F. Ali, M. Batool, J. Xiao and A. Irfan, Applications of UV/Vis Spectroscopy in Characterization and Catalytic Activity of Noble Metal Nanoparticles Fabricated in Responsive Polymer Microgels: A Review, *Crit. Rev. Anal. Chem.*, 2018, **48**, 503–516, DOI: 10.1080/10408347.2018.1451299.

26 P. Bhol and P. S. Mohanty, Smart microgel-metal hybrid particles of PNIPAM-co-PAA@AgAu: synthesis, characterizations and modulated catalytic activity, *J. Phys.: Condens. Matter*, 2020, **33**, 084002, DOI: 10.1088/1361-648X/abbe79.

27 L. Li, R. Niu and Y. Zhang, Ag–Au bimetallic nanocomposites stabilized with organic–inorganic hybrid microgels: synthesis and their regulated optical and catalytic properties, *RSC Adv.*, 2018, **8**, 12428–12438, DOI: 10.1039/C8RA01343H.

28 M. Ajmal, S. Demirci, M. Siddiq, N. Aktas and N. Sahiner, Simultaneous catalytic degradation/reduction of multiple organic compounds by modifiable p(methacrylic acid-co-

acrylonitrile)–M (M: Cu, Co) microgel catalyst composites, *New J. Chem.*, 2016, **40**, 1485–1496, DOI: 10.1039/C5NJ02298C.

29 K. Naseem, R. Begum, W. Wu, A. Irfan, A. G. Al-Sehemi and Z. H. Farooqi, Catalytic reduction of toxic dyes in the presence of silver nanoparticles impregnated core-shell composite microgels, *J. Cleaner Prod.*, 2019, **211**, 855–864, DOI: 10.1016/j.jclepro.2018.11.164.

30 Y. Lu, J. Yuan, F. Polzer, M. Drechsler and J. Preussner, *In situ* growth of catalytic active Au–Pt bimetallic nanorods in thermoresponsive core–shell microgels, *ACS Nano*, 2010, **4**, 7078–7086, DOI: 10.1021/nn102622d.

31 S. Saran, G. Manjari and S. P. Devipriya, Synergistic eminently active catalytic and recyclable Ag, Cu and Ag–Cu alloy nanoparticles supported on TiO$_2$ for sustainable and cleaner environmental applications: a phytogenic mediated synthesis, *J. Cleaner Prod.*, 2018, **177**, 134–143, DOI: 10.1016/j.jclepro.2017.12.181.

32 Z. H. Farooqi, S. Iqbal, S. R. Khan, F. Kanwal and R. Begum, Cobalt and nickel nanoparticles fabricated p(NIPAM-co-MAA) microgels for catalytic applications, *e-Polym.*, 2014, **14**, 313–321, DOI: 10.1515/epoly-2014-0111.

33 S. Jiang, H. Zhang, Y. Yan and X. Zhang, Stability and deactivation of Fe-ZSM-5 zeolite catalyst for catalytic wet peroxide oxidation of phenol in a membrane reactor, *RSC Adv.*, 2015, **5**, 41269–41277, DOI: 10.1039/C5RA05039A.

34 Y. Yang, H. Zhang and Y. Yan, Synthesis of CNTs on stainless steel microfibrous composite by CVD: effect of synthesis condition on carbon nanotube growth and structure, *Composites, Part B*, 2019, **160**, 369–383, DOI: 10.1016/j.compositesb.2018.12.100.

35 Y. Yang, H. Zhu, X. Xu, L. Bao, Y. Wang, H. Lin and C. Zheng, Construction of a novel lanthanum carbonate-grafted ZSM-5 zeolite for effective highly selective phosphate removal from wastewater, *Microporous Mesoporous Mater.*, 2021, **324**, 111289, DOI: 10.1016/j.micromeso.2021.111289.

36 Y. Yang, Y. Yan, H. Zhang and X. Wu, Catalytic wet peroxide oxidation of phenol on Fe-ZSM-5/PSSF membrane catalysts: effect of framework Fe by hydrothermal synthesis, *Sep. Purif. Technol.*, 2020, **237**, 116452, DOI: 10.1016/j.seppur.2019.116452.

37 M. U. Kakar, K. Khan, M. Akram, R. Sami, E. Khojah, I. Iqbal, M. Helal, A. Hakeem, Y. Deng and R. Dai, Synthesis of bimetallic nanoparticles loaded on to PNIPAM hybrid microgel and their catalytic activity, *Sci. Rep.*, 2021, **11**, 14759, DOI: 10.1038/s41598-021-94177-6.

38 Q. Sun, B. W. J. Chen, N. Wang, Q. He, A. Chang, C. M. Yang, H. Asakura, T. Tanaka, M. J. Hülsey, C. H. Wang, J. Yu and N. Yan, Zeolite-Encaged Pd–Mn Nanocatalysts for CO$_2$ Hydrogenation and Formic Acid Dehydrogenation, *Angew. Chem., Int. Ed.*, 2020, **59**, 20183–20191, DOI: 10.1002/anie.202008962.

39 B. Zhang, Y. Yuan, K. Philippot and N. Yan, Ag–Pd and CuO–Pd nanoparticles in a hydroxyl-group functionalized ionic liquid: synthesis, characterization and catalytic performance, *Catal. Sci. Technol.*, 2015, **5**, 1683–1692, DOI: 10.1039/c4cy01382d.

40 X. Yuan, G. Sun, H. Asakura, T. Tanaka, X. Chen, Y. Yuan, G. Laurenczy, Y. Kou, P. J. Dyson and N. Yan, Development of Palladium Surface-Enriched Heteronuclear Au–Pd Nanoparticle Dehalogenation Catalysts in an Ionic Liquid, *Chem.–Eur. J.*, 2013, **19**, 1227–1234, DOI: 10.1002/chem.201203605.

41 I. Hussain, F. Ali, M. Shahid, R. Begum, A. Irfan, W. Wu, S. Shaukat and Z. H. Farooqi, Silver nanoparticles supported on smart polymer microgel system for highly proficient catalytic reduction of Cr^{6+} to Cr^{3+} with formic acid, *Appl. Organomet. Chem.*, 2021, **35**, e6405, DOI: 10.1002/aoc.6405.

42 S. Iqbal, C. Zahoor, S. Musaddiq, M. Hussain, R. Begum, A. Irfan, M. Azam and Z. H. Farooqi, Silver nanoparticles stabilized in polymer hydrogels for catalytic degradation of azo dyes, *Ecotoxicol. Environ. Saf.*, 2020, **202**, 110924, DOI: 10.1016/j.ecoenv.2020.110924.

43 M. Arif, F. Tahir, U. Fatima, R. Begum, Z. H. Farooqi, M. Shahid, T. Ahmad, M. Faizan, K. Naseem and Z. Ali, Catalytic degradation of methyl orange using bimetallic nanoparticles loaded into poly(*N*-isopropylmethacrylamide) microgels, *Mater. Today Commun.*, 2022, 104700, DOI: 10.1016/j.mtcomm.2022.104700.

44 T. Zhang, L. Li, Z. Ye, Q. Yang, Y. Tian and X. Guo, Preparation and characterization of Ag–Pd bimetallic nano-catalysts in thermosensitive microgel nano-reactor, *RSC Adv.*, 2018, **8**, 18252–18259, DOI: 10.1039/c8ra02563k.

45 Y. Sha, I. Mathew, Q. Cui, M. Clay, F. Gao, X. J. Zhang and Z. Gu, Rapid degradation of azo dye methyl orange using hollow cobalt nanoparticles, *Chemosphere*, 2016, **144**, 1530–1535, DOI: 10.1016/J.Chemosphere.2015.10.040.

46 Y. Yang, H. Zhang and Y. Yan, Catalytic wet peroxide oxidation of *m*-cresol over novel Fe$_2$O$_3$ loaded microfibrous entrapped CNT composite catalyst in a fixed-bed reactor, *J. Chem. Technol. Biotechnol.*, 2018, **93**, 2552–2563, DOI: 10.1002/jctb.5609.

47 Y. Yang, H. Zhang, H. Huang, Y. Yan and X. Zhang, Iron-loaded carbon nanotube-microfibrous composite for catalytic wet peroxide oxidation of *m*-cresol in a fixed bed reactor, *Environ. Sci. Pollut. Res.*, 2020, **27**, 6338–6351, DOI: 10.1007/s11356-019-07362-6.

48 Y. Yang, K. Yuen Koh, R. Li, H. Zhang, Y. Yan and J. P. Chen, An innovative lanthanum carbonate grafted microfibrous composite for phosphate adsorption in wastewater, *J. Hazard. Mater.*, 2020, **392**, 121952, DOI: 10.1016/j.jhazmat.2019.121952.